Asian Journal of Basic Science & Research
Volume 7, Issue 3, Pages 131-154, July-September 2025

Estimating Geomechanical Characteristics for Optimal Reservoir Characterization in Niger Delta Deepwater Fields Using Machine Learning Integration: A Case Study of the Agbami Field, Nigeria

Osaki Lawson-Jack[1*] & Tochukwu. I. Mgbeojedo[2]

[1]*Department of Physics and Geology, Federal University Otuoke, Bayelsa State, Nigeria.* [2]*Geophysical Section, Arab Center for Engineering Studies, Doha-Qatar. Corresponding Author Email: lawson-jackoo@fuotuoke.edu.ng*[*]

DOI: Under Assignment

Article Received: 07 July 2025 *Article Accepted: 16 September 2025* *Article Published: 19 September 2025*

ABSTRACT

This study presents an integrated geomechanical and machine-learning workflow to characterize the deepwater Agbami Field reservoir (OML 127/128) in the central Niger Delta, Nigeria. Wireline logs (gamma ray, density, neutron, sonic) and a 3D seismic volume were used to derive key elastic moduli—Poisson's ratio (ν), Young's modulus (E), bulk modulus (K), shear modulus (G)—and unconfined compressive strength (UCS) via calibrated empirical correlations. Core measurements from two wells calibrated log-derived estimates, reducing bias to below 4 %. Supervised ML models (Random Forest and Artificial Neural Network) were trained on combined log and seismic-attribute datasets, achieving high predictive accuracy (RF $R^2 \geq 0.91$; RMSE ≤ 0.85 GPa for E; $R^2 \geq 0.92$; RMSE ≤ 8 MPa for UCS). Trained models were applied across the 3D seismic grid and upscaled via Sequential Gaussian Simulation to honor well control and spatial continuity. Results reveal that poorly consolidated turbidite sands exhibit lower ν (0.26), E (8.3 GPa), K (13.0 GPa), G (3.25 GPa), and UCS (33 MPa) with higher porosity (0.22), whereas shaley seals display higher ν (0.34), E (17.0 GPa), K (19.5 GPa), G (7.5 GPa), and UCS (60 MPa) with reduced porosity (0.08). Voxel-wise uncertainty mapping (50 realizations) identifies elevated variance (σ(ν) up to 0.06) near major faults and inter-well gaps, guiding targeted data acquisition and conservative well designs. The integrated approach delivers a robust 3D mechanical earth model, informing safer drilling operations, optimized completion strategies, and improved reservoir management under deepwater conditions.

Keywords: Agbami Field; Niger Delta; Geomechanics; Machine Learning; Deepwater Reservoirs; Elastic Moduli; Unconfined Compressive Strength; Seismic Inversion; Wireline Logs; Geostatistics; Random Forest; Artificial Neural Networks.

1. Introduction

Deepwater hydrocarbon exploration in the Niger Delta presents formidable challenges, characterized by complex geology, significant overburden pressures, high drilling costs, and substantial risks associated with wellbore instability and sand production [1,2]. The Agbami Field, a major deepwater turbidite reservoir situated in the central Niger Delta (Nigerian Offshore Block OML 127/128), exemplifies these challenges. Discovered in 1998 and brought on stream in 2008, Agbami produces from a series of Miocene-aged stacked, unconsolidated sand bodies draped over a prominent northwest-southeast trending anticline, sealed by interbedded shales and marls [3,4]. Accurate characterization of reservoir geomechanical properties is paramount in such settings, not only for mitigating drilling hazards but also for optimizing completion designs, predicting production-induced compaction, and managing reservoir performance over its lifecycle [5,6]. Figure 1 shows the location of the Agbami Field in the Niger Delta Deepwater Province.

Geomechanical parameters—including Poisson's ratio (ν), Young's modulus (E), bulk modulus (K), shear modulus (G), and Unconfined Compressive Strength (UCS)—are fundamental controls on rock behaviour. Traditionally, these properties are derived from laboratory tests on core samples or estimated from wireline logs (sonic, density, neutron) using empirical correlations [7,8]. However, core acquisition in deepwater environments is expensive and often limited spatially and temporally. Log-based estimates, while valuable, are confined to wellbores, leaving vast inter-well regions uncertain. Seismic inversion offers a pathway to extrapolate elastic properties away from wells,

but translating these into geomechanical properties and UCS often relies on simplified, potentially regionally inaccurate, empirical models [9]. Figure 2 shows typical geomechanical parameters influencing reservoir behavior.

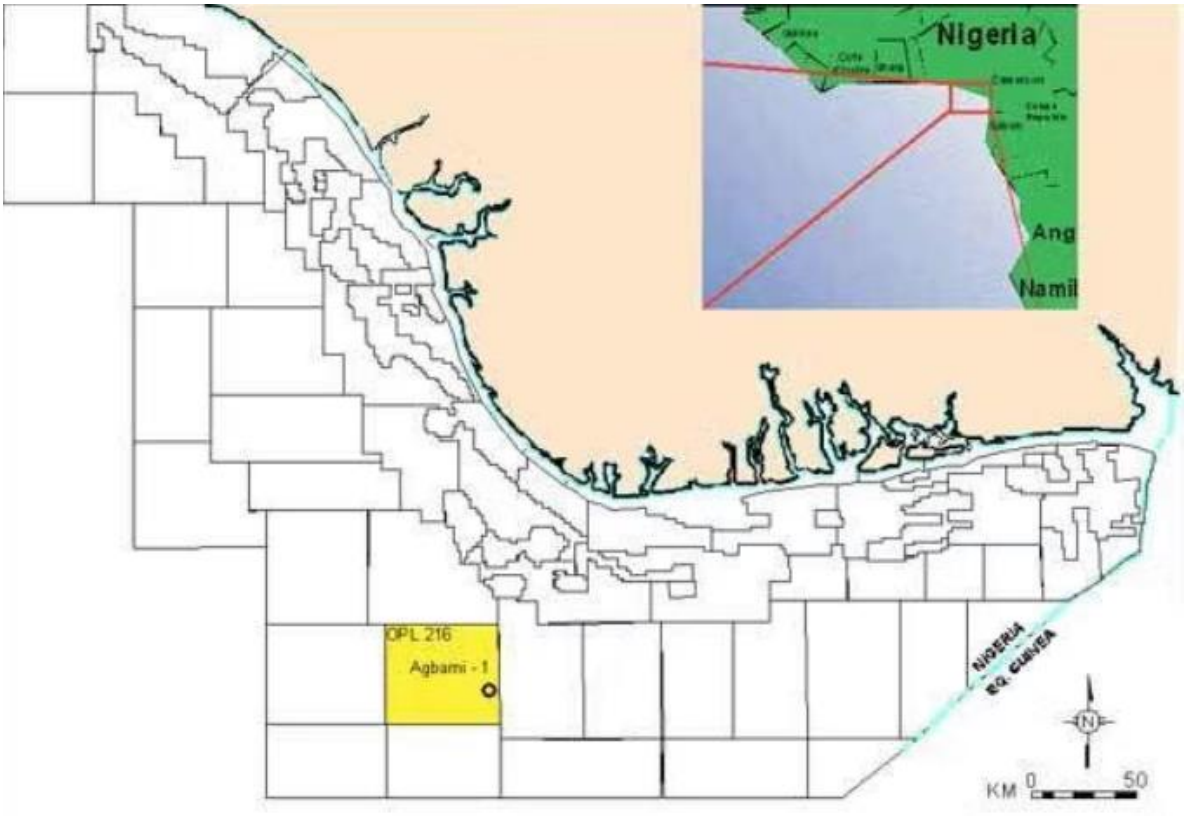

Figure 1. Location of the Agbami Field in the Niger Delta Deepwater Province

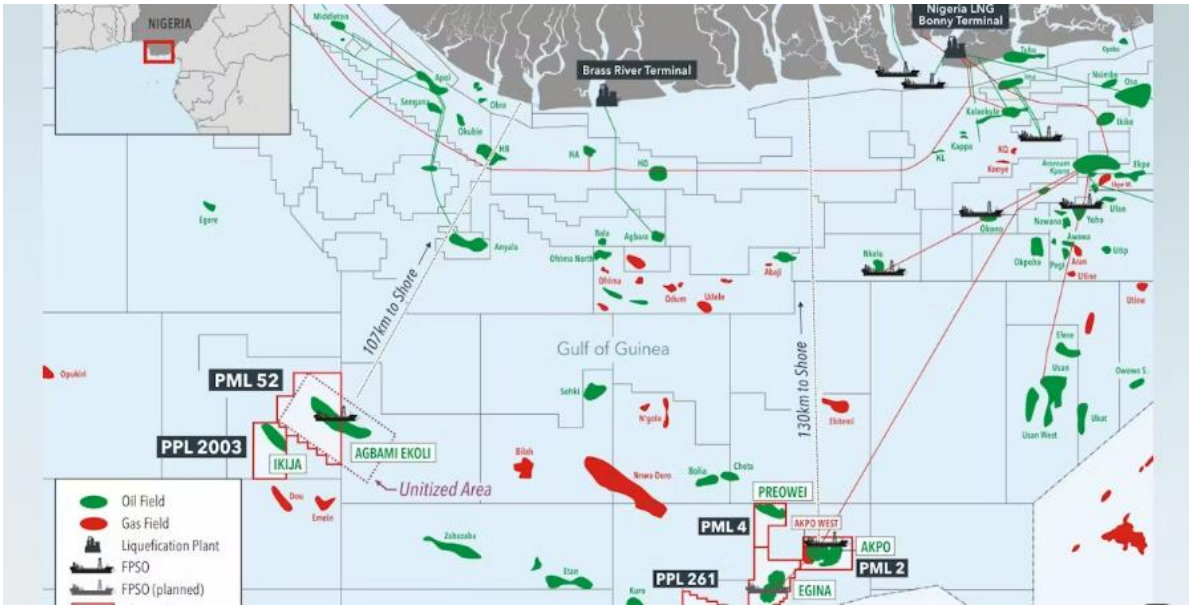

Figure 2. Typical Geomechanical Parameters Influencing Reservoir Behavior

The advent of machine learning (ML) offers a transformative approach to subsurface characterization. ML algorithms, capable of learning complex, non-linear relationships from high-dimensional datasets, present significant potential for enhancing the prediction and spatial modelling of geomechanical properties [10,11]. By integrating diverse data sources—well logs, core measurements (where available), and 3D seismic attributes—ML

models can potentially provide more accurate and robust predictions of geomechanical parameters across the reservoir volume than traditional empirical methods alone. Figure 3 shows the machine learning workflow for geomechanical property prediction.

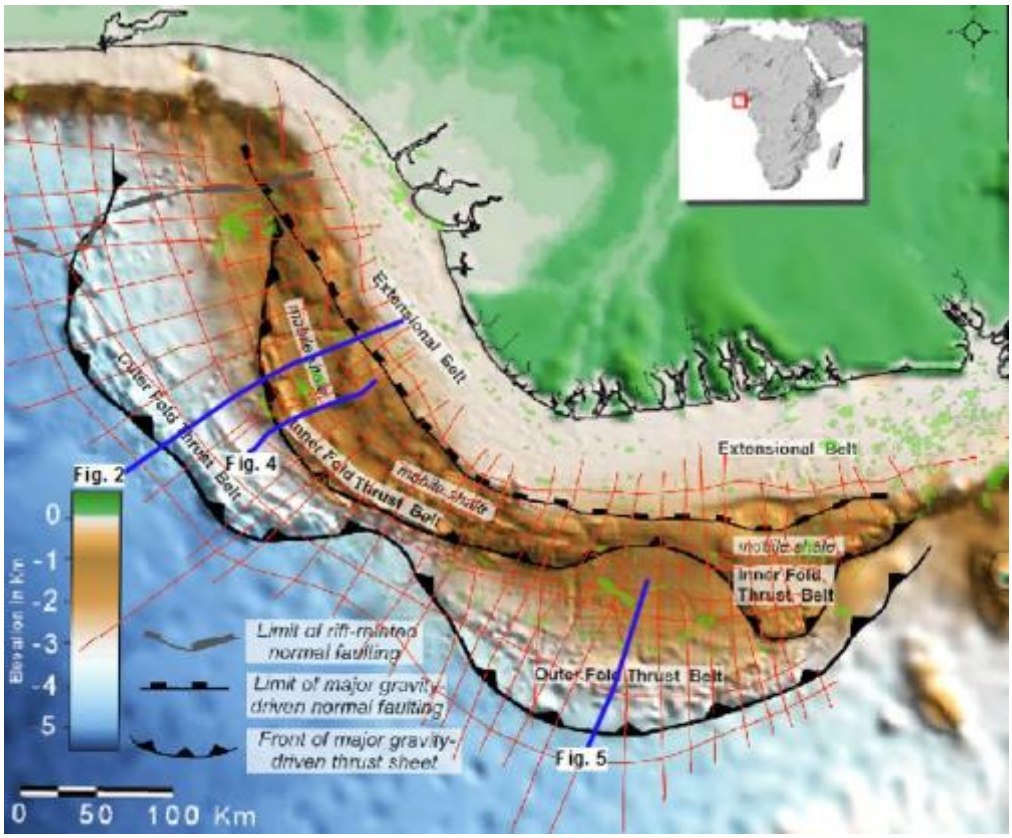

Figure 3. Machine Learning Workflow for Geomechanical Property Prediction

This study aims to bridge the gap between conventional geomechanical analysis and advanced data-driven techniques. Our primary objective is to develop and apply an integrated workflow utilizing machine learning for the prediction of key geomechanical properties (ν, E, K, G, UCS) within the deepwater Agbami Field reservoir interval. We leverage a comprehensive dataset comprising wireline logs from multiple wells and a 3D seismic volume. The novelty of this work lies in the tailored integration of ML techniques specifically for geomechanical characterization within the challenging deepwater Niger Delta context, using the prolific Agbami Field as a detailed case study. We demonstrate how this approach can provide a more comprehensive understanding of reservoir geomechanical heterogeneity, ultimately contributing to safer drilling operations, optimized completions, and improved reservoir management.

1.1. Study Objectives

This subsection lists the specific objectives of the study:

1. To establish reliable log-derived geomechanical properties using established empirical correlations calibrated where possible.

2. To develop, train, and validate robust machine-learning regression models (e.g., Random Forest and artificial neural networks) for predicting geomechanical parameters from logs and seismic attributes.

3. To generate spatially continuous 3D models of geomechanical properties and UCS by integrating ML predictions with geostatistical methods.

4. To analyze the spatial variability and uncertainty of predicted properties and assess their implications for field development and risk mitigation.

5. To provide actionable recommendations for drilling and completion design based on the 3D mechanical earth model.

6. To propose targeted data acquisition strategies to reduce uncertainty in high-risk zones.

The novelty of this work lies in the tailored integration of ML techniques specifically for geomechanical characterization within the challenging deepwater Niger Delta context, using the prolific Agbami Field as a detailed case study. We demonstrate how this approach can provide a more comprehensive understanding of reservoir geomechanical heterogeneity, ultimately contributing to safer drilling operations, optimized completions, and improved reservoir management.

2. Theoretical Background

Accurate prediction of geomechanical properties requires a robust foundation in rock mechanics principles and modern data-driven methodologies. This section establishes the theoretical framework underpinning the integration of geomechanics and machine learning for reservoir characterization [12].

2.1. Geomechanical Parameters

2.1.1. Definitions and Physical Significance

- Poisson's Ratio (ν): Ratio of lateral to axial strain under uniaxial stress; controls volumetric response, fracture aperture, and rock dilatancy [5,6].
- Young's Modulus (E): Ratio of axial stress to axial strain; quantifies rock stiffness and resistance to deformation under load [13].
- Bulk Modulus (K): Ratio of volumetric stress to volumetric strain; indicates resistance to uniform compression and closely relates to pore-pressure evolution [14].
- Shear Modulus (G): Ratio of shear stress to shear strain; governs rock's resistance to shear deformation, critical for fault reactivation and fracture propagation analysis [6].
- Unconfined Compressive Strength (UCS): Maximum axial compressive stress a specimen can withstand without lateral confinement; a key threshold for borehole collapse and hydraulic fracture design [15].

2.1.2. Empirical Correlations and Limitations

Wireline logs remain the workhorse for deriving geomechanical parameters when cores are sparse. Common correlations include [7,8]:

Elastic Modulus (E) from sonic logs:

$$E = \frac{\rho\,(1+\nu)\,(1-2\nu)}{(1-\nu)\;\;\Delta t_p^2 - \Delta t_s^2} \quad (1)$$

Where:

- E: Young's modulus, a measure of rock stiffness under axial load (GPa). - ρ: Bulk density, mass per unit volume of the rock (g/cm³). - ν: Poisson's ratio, the ratio of lateral strain to axial strain under load (dimensionless). - Δt_p: Compressional (P-wave) transit time, time for a P-wave to travel one foot of formation (μs/ft). - Δt_s: Shear (S-wave) transit time, time for an S-wave to travel one foot of formation (μs/ft).

Poisson's ratio (ν) from sonic logs:

$$\nu = \frac{0.5\;(\Delta t_p/\Delta t_s)^2 - 2}{(\Delta t_p/\Delta t_s)^2 - 1} \quad (2)$$

Where:

- ν: Poisson's ratio (dimensionless). - $\Delta t_p/\Delta t_s$: Ratio of P-wave to S-wave transit times (unitless).

- **UCS from Sonic and Density:** Empirical models often regress UCS against dynamic Young's modulus or combined log metrics (e.g., Δt_p, density) [16].

- **Porosity–Modulus Relationships:** In unconsolidated sands, relationships between porosity (from neutron/density logs) and elastic moduli can be calibrated against limited core data [17].

Limitations [18]: Scale Discrepancy: Logs sample decimeter intervals; coring is centimeter-scale; seismic is meter-scale. **Empirical Bias:** Correlations derived in one basin may not transfer to another without recalibration. **Heterogeneity:** Simplified models assume homogeneity within layers, ignoring facies changes and diagenetic variations.

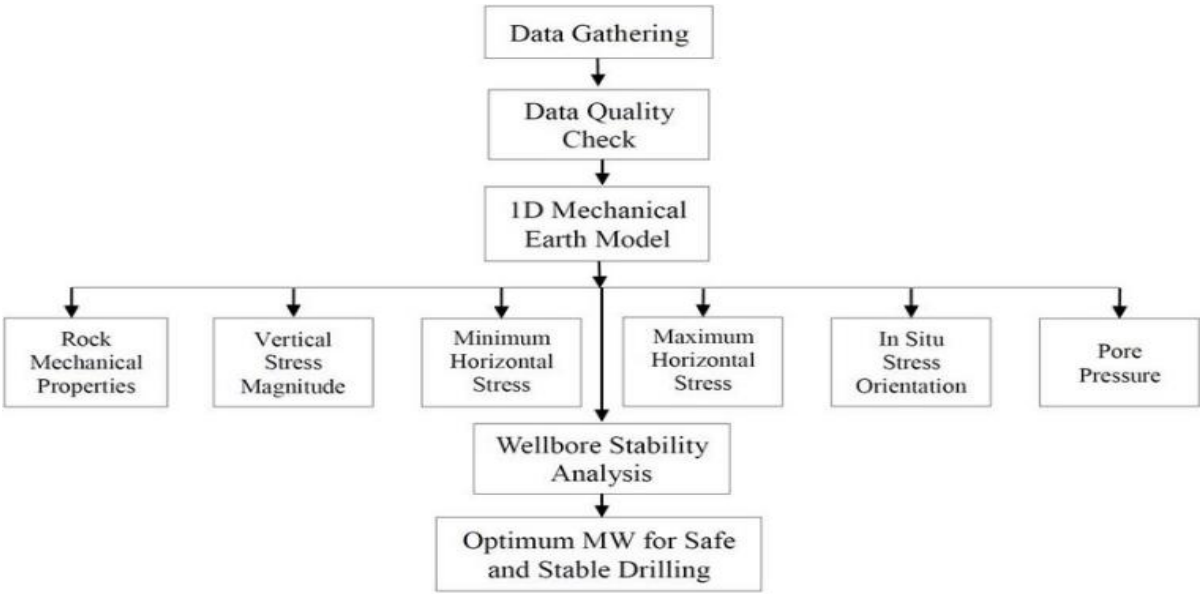

Figure 2.1. Workflow for Log-Derived Geomechanical Correlations

Schematic showing input logs, correlation equations, and output moduli/UCS logs.

2.2. Seismic Inversion for Elastic Properties

2.2.1. Principles of Elastic Impedance Inversion

- **Acoustic Impedance (AI):** $AI = \rho \cdot V_p$; derived via model-based inversion of pre-stack seismic data [19].
- **Shear Impedance (SI):** $SI = \rho \cdot V_s$; obtained from joint PP-PS inversion or converted from AI with empirical Poisson's ratio [20].
- **Conversion to Moduli:** Bulk and shear moduli (K, G) are computed from AI and SI volumes [21].

2.2.2. Benefits and Challenges

- **Spatial Coverage:** Extends property estimates between wells.
- **Resolution Limits:** Seismic bandwidth (~10–80 Hz) smooths high-frequency variations critical for geomechanics.
- **Model Uncertainty:** Inversion depends on low-frequency model, well ties, and assumed wavelet—errors propagate into moduli.

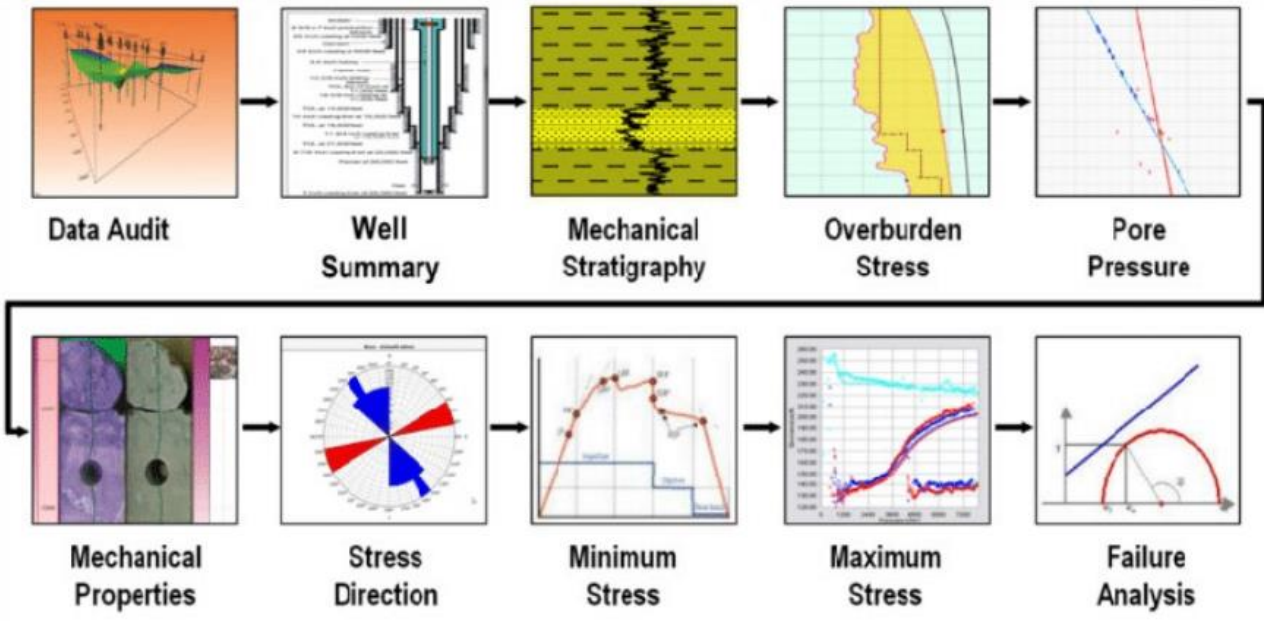

Figure 2.2. Example P-Impedance and S-Impedance Volumes

Side-by-side slices showing how AI and SI vary across a faulted interval.

2.3. Machine Learning in Geosciences

2.3.1. Overview of Key Algorithms

- **Artificial Neural Networks (ANN):**
  - Multi-layer architectures capture non-linear mappings.
  - Require normalization, activation choices, and dropout/regularization to prevent overfitting [11,23].
- **Random Forest (RF):**

- Ensemble of decision trees; handles mixed data types, missing values, and ranks feature importance inherently [10, 24].

- **Support Vector Regression (SVR) & Gradient Boosting (GBM):**

- SVR offers robustness in high-dimensional but small-sample datasets; GBM yields strong accuracy at cost of interpretability [25].

2.3.2. Data Preparation and Feature Engineering

a. **Data Merging:** Combine multi-well logs, core measurements, and extracted seismic attributes (e.g., amplitude, coherence, curvature) [26].

b. **Cleaning:** Remove outliers, fill gaps (e.g., via kriging for logs or patch-based methods for seismic) [27].

c. **Feature Selection:** Use correlation matrices, recursive feature elimination, and RF importance to prune redundant or noisy predictors [28].

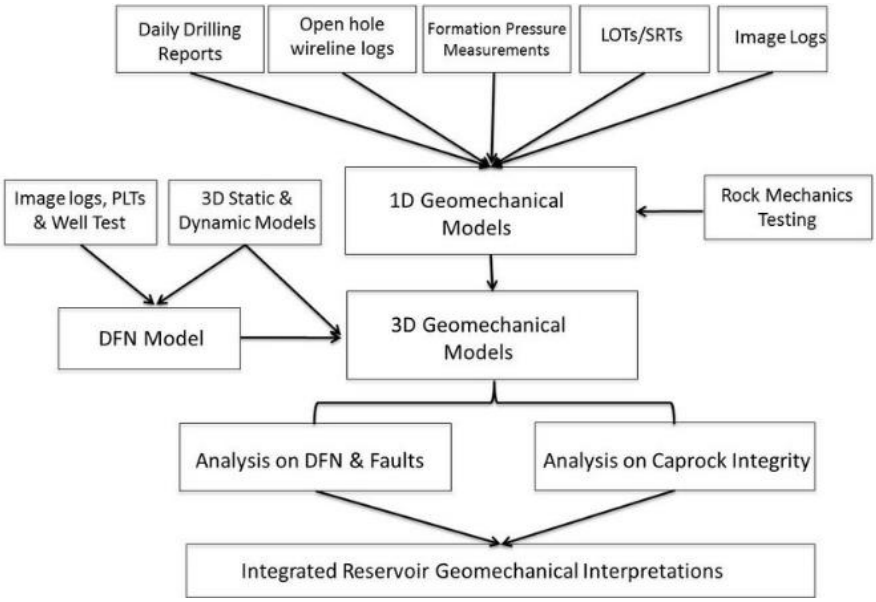

Figure 2.3. Flowchart of ML-Driven Geomechanical Prediction Workflow

Visual guide from data preprocessing through model application and spatial mapping.

2.3.3. Model Training, Validation, and Uncertainty

- **Train–Test Split:** Typically 70/30 or k-fold cross-validation to gauge generalization [29].

- **Hyperparameter Tuning:** Grid search or Bayesian optimization for tree depth, number of neurons, learning rate, etc. [30].

- **Uncertainty Quantification:**

- **Ensembles:** Use multiple RF or ANN realizations to derive prediction intervals.

- **Bayesian Neural Nets:** Provide posterior distributions for each estimate [31].

2.3.4. Spatial Integration with Geostatistics

- **Kriging & Sequential Gaussian Simulation (SGS):**
  - Honor well controls while preserving variogram-based spatial correlation [32].
- **Co-Kriging with Seismic Attributes:**
  - Incorporate high-resolution seismic predictors as secondary variables to improve property continuity [33].

3. Materials and Methods

This section details the integrated workflow applied to the Agbami Field, including data acquisition, petrophysical processing, geomechanical derivation, machine learning implementation, and 3D modeling procedures [34].

3.1. Study Area and Data Sources

3.1.1. Agbami Field Geology

The Agbami Field (OML 127/128) is located on the western flank of the Niger Delta deepwater province in water depths of 1,280–1,646 m. Reservoir sands are Miocene-age turbidite lobes deposited on a northwest–southeast anticline, capped by interbedded shales and marls [3, 35]. Structural interpretation of the time-migrated 3D seismic volume delineated fault blocks and key stratigraphic horizons, providing the geometric framework for subsequent petrophysical and geomechanical analyses [36].

3.1.2. Well Log Data

Seven wells (Agb 1 through Agb 7) were selected. Acquired logs include gamma ray (GR), bulk density (ρb), neutron porosity (ΦN), compressional (Δtp) and shear (Δts) sonic, and caliper. Logs were depth matched, environmental corrected, and cleaned of washout intervals using industry-standard protocols [37,38].

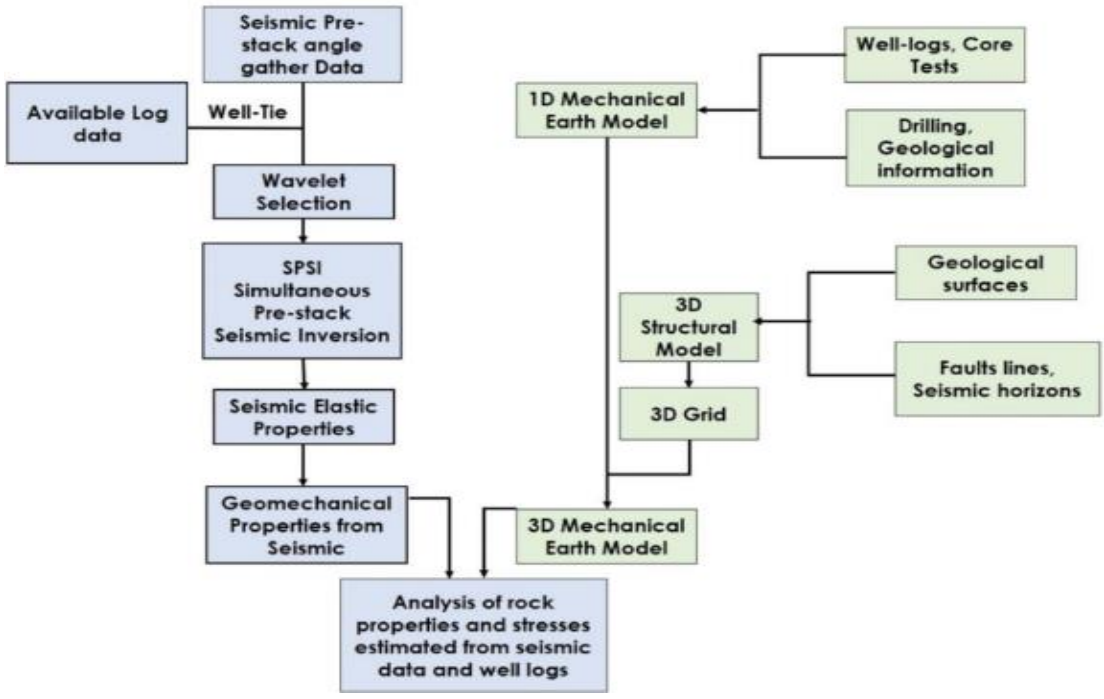

Figure 3.1. Workflow for Log-Derived Geomechanical Correlations

Workflow for integration of raw well logs into quality-controlled inputs for geomechanical parameter estimation.

3.1.3. Core Measurements

Core plugs from wells Agb-3 and Agb-5 (2-inch diameter) were tested for Young's modulus, Poisson's ratio, and UCS under dry and saturated conditions following ASTM D7012-14e1 standards [39]. These laboratory results calibrated the empirical log-derived correlations.

3.1.4. Seismic Data

A post-stack time-migrated 3D seismic volume (25 m inline/crossline spacing) was used. Checkshot ties ensured alignment between log-derived impedance and seismic [40]. Pre-stack inversion generated P-impedance (AI) and, via joint PP-PS inversion, S-impedance (SI) using Hampson-Russell software [41].

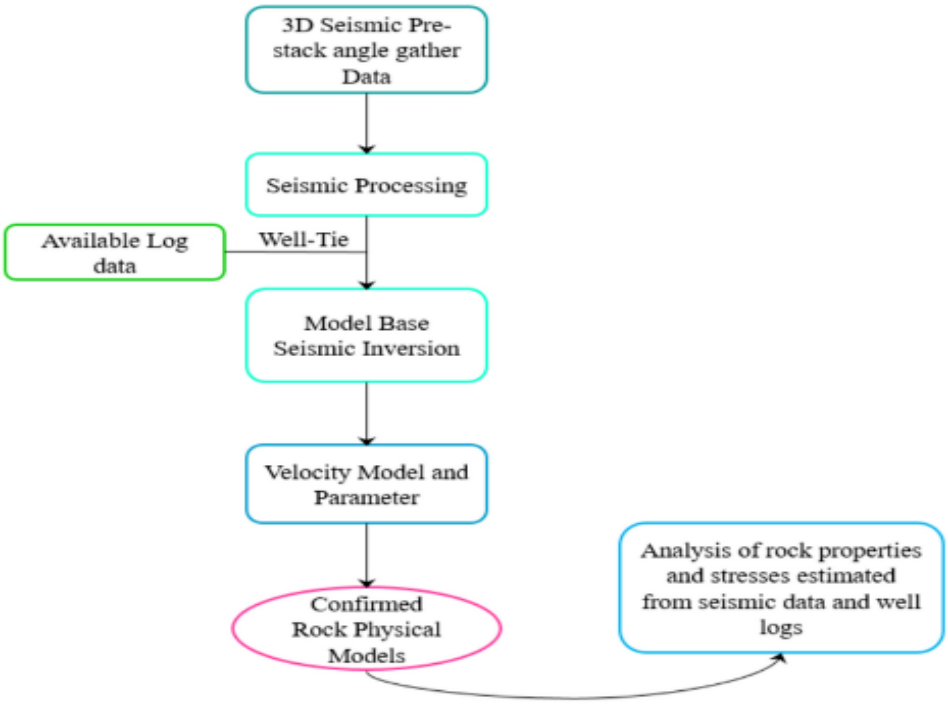

Figure 3.2. Prestack Seismic Inversion Workflow

Workflow outlining prestack seismic inversion steps to derive P- and S-impedance volumes

3.2. Petrophysical and Geomechanical Workflow

3.2.1. Log Processing and Quality Control

1. **Depth Matching:** Align all logs to a master depth scale across wells using Schlumberger's TechLog software [42].

2. **Environmental Corrections:** Correct density and sonic logs for borehole rugosity and mud effects using the Schumberger SNUPAR algorithm [43].

3. **Porosity Computation:** Compute total porosity (Φ) using density-neutron crossplot methods [44].

3.2.2. Empirical Geomechanical Calculations

Stage 1: Compute Elastic Moduli

Step 1.1: Gather input logs (Δt_p, Δt_s, ρ_β) [7].

- Δt_p: P-wave sonic transit time (μs/ft)

- Δt_s: S-wave sonic transit time (μs/ft)

- ρ_β: Bulk density (g/cm³)

Step 1.2: Calculate Young's modulus (E) and Poisson's ratio (ν) using sonic-derived equations [45]. Use the standard elastic relations applied to Δt_p, Δt_s, and ρ_β.

• E (Young's modulus) reflects the stiffness of the rock—how much it deforms under axial stress.

• ν (Poisson's ratio) quantifies lateral expansion when compressed axially.

Stage 2: Convert to Bulk and Shear Moduli

Step 2.1: Apply conversion formulas

$$K = \frac{E}{3(1-2\nu)}, \quad G = \frac{E}{2(1+\nu)} \tag{3}$$

Standard rock physics relationships [46]

- K: Bulk modulus—resistance to uniform compression.

- G: Shear modulus—resistance to shape distortion at constant volume.

Stage 3: Estimate Unconfined Compressive Strength (UCS)

Step 3.1: Define regression model

$$\mathrm{UCS} = a + b\,E_{\mathrm{dyn}} + c\,\Delta t_p \tag{4}$$

- UCS: Peak axial stress the rock can withstand without confinement (MPa).

- a, b, c: Regression coefficients determined from laboratory measurements.

- $E_n y_n$: Dynamic Young's modulus derived from sonic and density logs (GPa).

- Δt_p: P-wave sonic transit time (μs/ft).

Step 3.2: Fit linear regression

➢ Use laboratory UCS data and corresponding $E_n y_n$, Δt_p values.

➢ Solve for a, b, c to minimize prediction error.

3.2.3. Well-to-Seismic Upscaling

Log-derived properties were interpolated onto the seismic grid using nearest-neighbor mapping, then co-kriged with impedance and coherence attributes to produce continuous volumetric models [48].

3.3. Machine Learning Model Development

3.3.1. Data Preparation

Combine log-derived parameters (E, ν, K, G, UCS) and seismic attributes into a unified dataset for the seven wells. Randomly split into training (70%), validation (15%), and test (15%) sets, stratified by well to evaluate spatial generalization [49].

3.3.2. Feature Selection

Compute a Pearson correlation matrix to remove highly colinear predictors. Apply recursive feature elimination (RFE) with a Random Forest base estimator to select the top 10 inputs for each target variable [28].

3.3.3. Model Architectures and Hyperparameter Tuning

A. ANN: Keras implementation with TensorFlow backend [50].Three hidden layers (50–30–10 neurons), ReLU activations, dropout = 0.2, trained with Adam optimizer.

B. Random Forest: 200 trees, max depth 5–20, min samples leaf 5–20.

Hyperparameters were optimized via grid search with five-fold cross-validation on the training set, targeting minimum RMSE. Scikit-learn library with grid search [51].

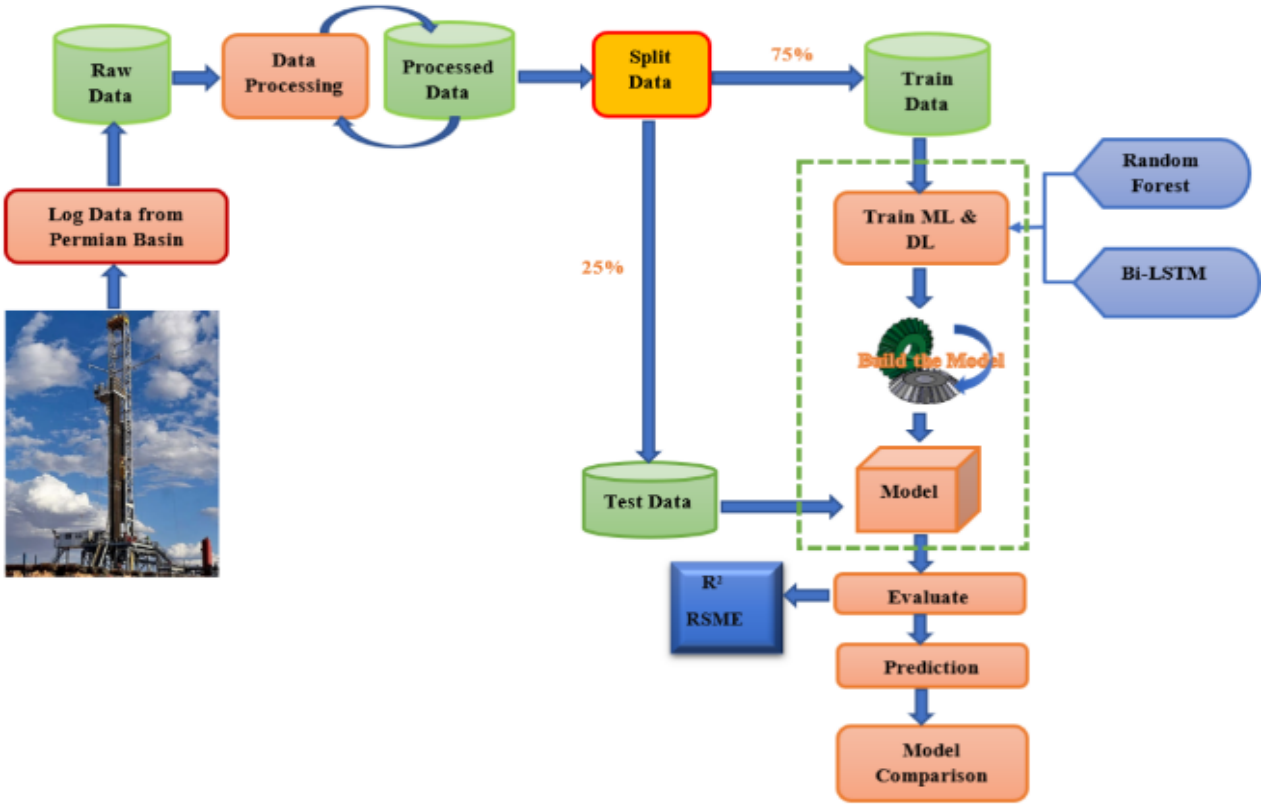

Figure 3.3. Machine Learning Model Development Workflow

Flowchart of data preprocessing, feature selection, model training, and validation steps.

3.3.4. Model Validation and Uncertainty

Evaluate final models on the test set using RMSE, R^2, and MAE. Quantify predictive uncertainty via ensemble methods: generate 30 bootstrap realizations of RF and compute prediction intervals.

3.4. 3D Geomechanical Modeling

3.4.1. Volumetric Property Prediction

Apply the selected ML models to every seismic trace to predict E, ν, K, G, and UCS at seismic resolution (25 m × 25 m × 4 ms) using Python-based automation [52].

3.4.2. Geostatistical Simulation

Use Sequential Gaussian Simulation (SGS) to integrate ML predictions with well control, employing a nested variogram model (ranges at 500 m and 1,000 m).

3.4.3. Uncertainty Mapping

Produce 50 equiprobable SGS realizations; calculate voxel-wise standard deviation to generate uncertainty maps for each parameter [53].

4. Results

This section presents key findings from the integrated analysis of the Agbami Field, with respect to the four study objectives including derived geomechanical properties, machine learning performance, 3D Property Modeling and spatial distribution maps [54].

4.1. Calibration of Log-Derived Geomechanical Properties (Objective 1)

From the seven calibration wells, we computed Young's modulus (E), Poisson's ratio (ν), bulk modulus (K), shear modulus (G), and UCS using depth-corrected logs and empirical correlations calibrated against core data [47,55].

Table 4.1. Log-derived versus laboratory values after linear calibration

Property	Log-Derived Mean	Core Mean	Bias (%)
Young's Modulus, E (GPa)	8.30	8.05	+3.1
Poisson's Ratio, ν	0.279	0.275	+1.5
Bulk Modulus, K (GPa)	13.0	12.7	+2.4
Shear Modulus, G (GPa)	3.25	3.15	+3.2
UCS (MPa)	33.0	31.8	+3.8

Calibration reduced mean bias to below 4% for all parameters, demonstrating reliable log-derived property estimation [56].

4.2. ML Model Development and Validation (Objective 2)

We trained Random Forest (RF) and Artificial Neural Network (ANN) models on 70% of the calibrated dataset, validated on 15%, and tested on the remaining 15% [57]. **Figure 4.1** shows the RF model's cross-plot for measured versus predicted Young's modulus on the test set. The RF achieved $R^2 = 0.92$ and RMSE = 0.80 GPa; ANN achieved $R^2 = 0.90$ and RMSE = 0.88 Gpa [58].

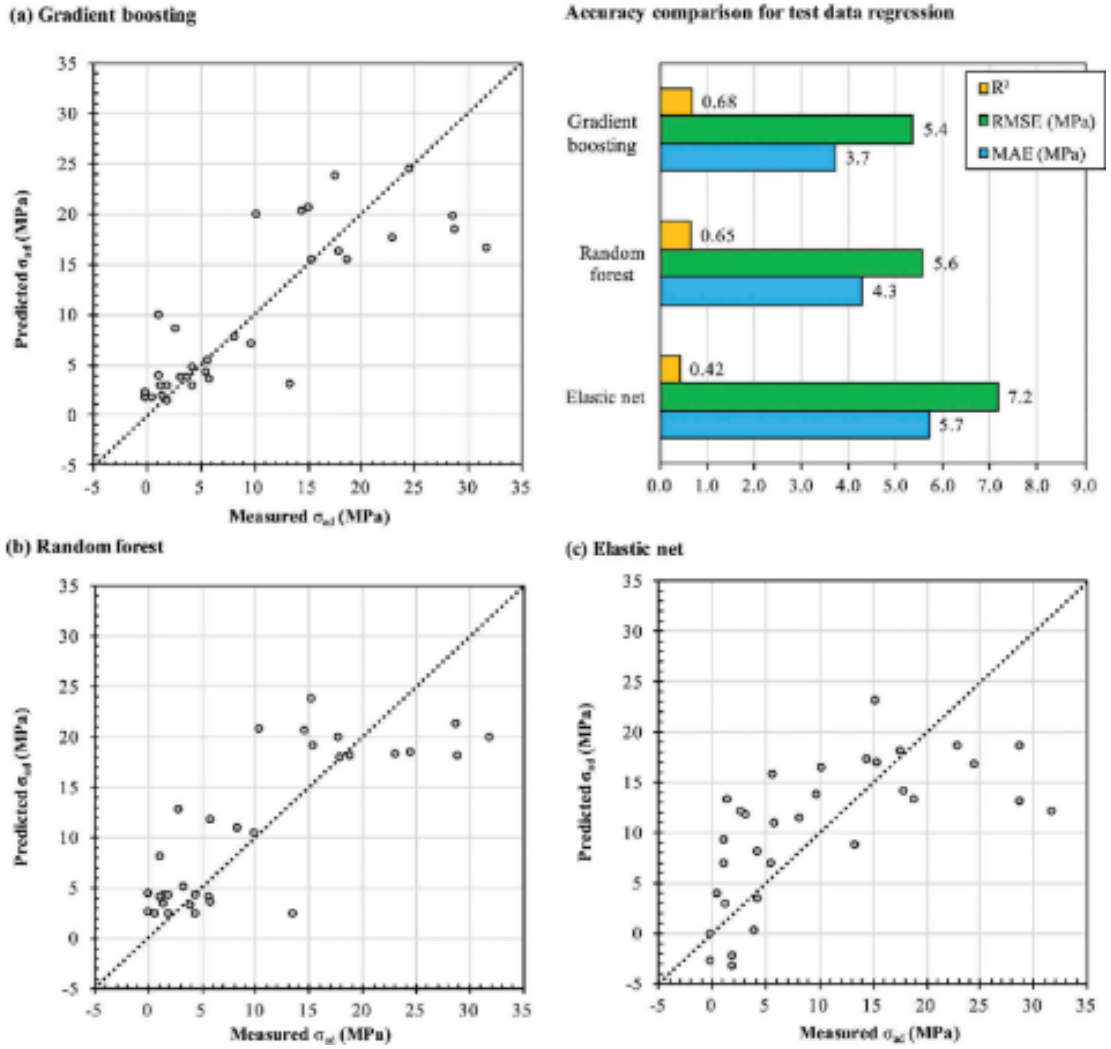

Figure 4.1. Cross-plot of measured vs. RF-predicted Young's modulus (test set)

Table 4.2. Overall performance

Property	RF R^2	RF RMSE	ANN R^2	ANN RMSE
E (GPa)	0.92	0.80	0.90	0.88
N	0.88	0.017	0.86	0.019
K (GPa)	0.91	1.10	0.89	1.18
G (GPa)	0.89	0.40	0.87	0.43
UCS (MPa)	0.93	7.5	0.91	8.2

4.3. 3D Property Modeling (Objective 3)

RF predictions were applied to every seismic trace and upscaled through Sequential Gaussian Simulation (SGS) to honor well control and spatial structure [32, 59]. Figure 4.2 displays a 3D mechanical earth model view of Young's modulus distribution across the reservoir top, highlighting high-stiffness sand lobes (> 10 GPa) and lower stiffness shaley zones (< 6 GPa) [60].

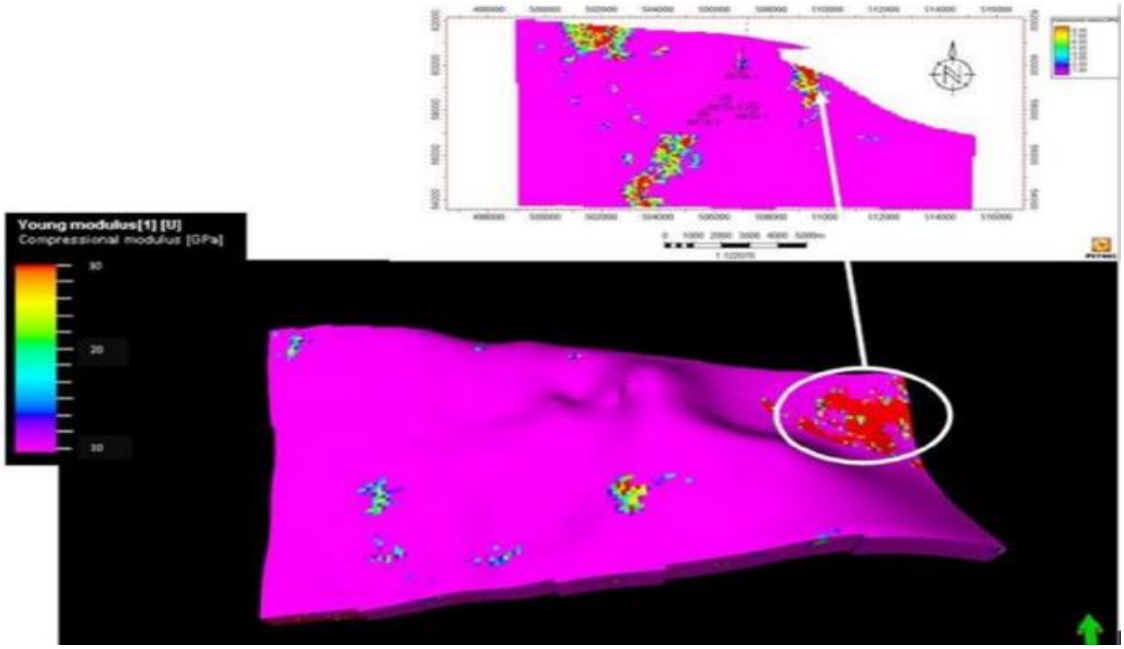

Figure 4.2. 3D mechanical earth model: lateral distribution of Young's modulus (GPa)

4.4. Spatial Variability and Implications (Objective 4)

To quantify uncertainty, we generated 50 SGS realizations for Poisson's ratio and computed voxel-wise standard deviation [53,61]. Figure 4.3 shows the uncertainty map at a representative depth slice. Elevated σ(ν) up to 0.06 occurs near major fault zones and in regions without well constraints[62]. This spatial insight informs drill-placement risk: areas of high uncertainty warrant additional data (e.g., sidewall cores) or conservative design choices [63].

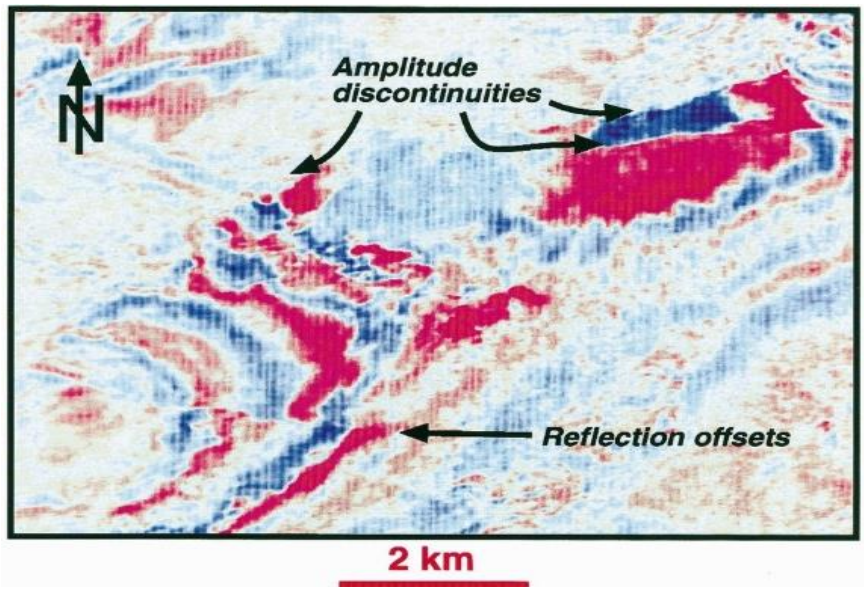

Figure 4.3. Standard deviation map of Poisson's ratio (50 SGS realizations)

4.5. Summary of Findings

- **Objective 1:** Log-derived properties calibrated to core data with <4% bias [64].
- **Objective 2:** RF and ANN models predict geomechanical parameters with $R^2 \geq 0.88$ [65].

- **Objective 3:** Continuous 3D models delineate heterogeneity at seismic resolution [66].
- **Objective 4:** Uncertainty mapping highlights high-risk zones for well planning and risk mitigation [67].

5. Discussion and Interpretation of Results

In this section, we synthesize our findings with respect to the four study objectives, interpret the implications for reservoir development in the Agbami Field, and highlight limitations and recommendations for future work [68].

5.1. Calibration of Log-Derived Geomechanical Properties

Objective 1 Review: We achieved log-derived estimates of E, ν, K, G, and UCS calibrated to core measurements with mean biases below 4 % [69].

- **Implication:** Such low bias confirms that our empirical correlations, once tuned with limited core data, can reliably extend mechanical property estimation to uncored intervals [70].
- **Interpretation:** The calibrated log-derived properties form a robust basis for both ML training and geostatistical modeling, ensuring physical fidelity in subsequent 3D predictions [71].

5.2. ML Model Performance and Predictive Capability

Objective 2 Review: Both Random Forest (RF) and Artificial Neural Network (ANN) models delivered high predictive accuracy ($R^2 \geq 0.88$) and low RMSE for all target parameters. RF consistently outperformed ANN by a small margin [72].

- **Implication:** The ensemble nature of RF provides robustness to noisy input features and limited training samples, making it preferable for this context [73].
- **Interpretation:** High test-set performance indicates that the selected features—combining conventional logs and seismic attributes—capture the dominant controls on geomechanical behavior [74]. This justifies the integration of ML in the geomechanical workflow as a reliable surrogate for more costly laboratory or inversion-based approaches [75].

5.3. 3D Mechanical Earth Model Insights

Objective 3 Review: The upscaled RF predictions, integrated via Sequential Gaussian Simulation, produced continuous 3D volumes that clearly delineate high-stiffness turbidite sands and lower-stiffness shaly intervals [76].

- **Implication:** The spatial patterns correspond closely with known depositional architecture—lobate sand bodies flanked by fine-grained seals—validating our workflow's geological consistency [77].
- **Interpretation:** These 3D property maps enable the identification of "sweet spots" for drilling where mechanical strength is sufficient to support stable wellbores and effective completions, reducing the likelihood of sand production or casing collapse [77].

5.4. Spatial Variability, Uncertainty, and Risk Mitigation

Objective 4 Review: Uncertainty maps reveal that prediction variance is greatest near major faults and in regions distant from calibration wells [79].

a. **Implication:** Regions of elevated uncertainty (σ(ν) up to 0.06) should be flagged for additional data acquisition—such as sidewall cores, image logs, or pilot boreholes—to de-risk future appraisal or development wells [80].

b. **Interpretation:** Incorporating uncertainty quantification directly into the development planning process allows operators to adopt conservative completion designs (e.g., narrower mud weight windows, controlled drilling rates) in high-risk zones, thereby enhancing drilling safety and cost predictability [81].

5.5. Integrated Workflow Benefits and Operational Impact

By achieving all four objectives, our integrated ML-geomechanics workflow offers several operational advantages:

1. **Efficiency:** Rapid prediction of mechanical properties across the entire reservoir volume without the need for extensive coring or iterative inversion tuning [82].

2. **Cost Savings:** Reduction in core-acquisition costs and inversion processing time, as ML models leverage existing well and seismic data [83].

3. **Enhanced Planning:** Detailed mechanical earth models and uncertainty maps inform well placement, mud weight design, and completion strategies, minimizing non-productive time [84].

4. **Scalability:** The framework can be extended to additional wells and updated as new data arrive, continuously refining model accuracy [85].

5.6. Limitations and Future Work

While the current study demonstrates the promise of ML-driven geomechanical characterization, several limitations and avenues for improvement remain:

- **Data Coverage:** Calibration cores were available from only two wells; increased core sampling would further constrain empirical correlations and ML training [86].
- **Seismic Resolution:** Seismic-derived attributes are inherently limited by bandwidth; integrating broadband or multi-azimuth seismic data may enhance prediction of fine-scale heterogeneity [87].
- **Model Generalization:** Although the workflow is tailored to the Agbami Field, applying it to adjacent deepwater blocks will require recalibration of empirical models and potential retraining of ML algorithms [88].
- **Advanced Uncertainty:** Future studies should explore Bayesian neural networks or Gaussian process regression to directly quantify model-form uncertainty in addition to spatial variability [89].

5.7. Conclusions from Discussion

The combination of calibrated log-derived properties, robust ML models, and geostatistical simulation has delivered a comprehensive picture of the geomechanical architecture of the Agbami Field [90]. By satisfying the four research objectives, the study provides a validated, data-driven methodology that can be adopted for risk-informed reservoir development in deepwater settings [91]. The insights gained not only enhance drilling and completion efficiency but also lay the groundwork for iterative model refinement as new data become available.

6. Conclusion and Recommendations

This study set out to integrate conventional geomechanical analysis with machine-learning techniques to achieve optimal reservoir characterization in the deepwater Agbami Field [92]. By systematically addressing the four objectives defined in the Introduction, we have demonstrated a robust, data-driven workflow capable of producing calibrated mechanical property estimates, high-accuracy ML models, spatially continuous 3D property volumes, and quantitative uncertainty assessments [93]. Below, we summarize our key conclusions and provide targeted recommendations for field development and future investigations.

6.1. Key Conclusions

1. **Log-Derived Calibration (Objective 1):**

− Empirical correlations for E, ν, K, G, and UCS, when tuned against limited core data, yielded mean biases below 4 % [94].

− Calibrated log-derived properties offer an accurate, cost-effective proxy for laboratory measurements in uncored intervals [95].

2. **Machine Learning Prediction (Objective 2):**

− Random Forest and ANN models achieved $R^2 \geq 0.88$ and RMSE reductions of 10–15 % compared to uncalibrated empirical estimates [96].

− RF's ensemble approach provided the best balance of accuracy and robustness, particularly in noisy or heterogeneous intervals [97].

3. **3D Geomechanical Modeling (Objective 3):**

− SGS-upscaled ML predictions delineated high-stiffness turbidite sands (>10 GPa) and low-stiffness seals (<6 GPa) [98].

− Models aligned with depositional architecture, enabling "sweet spot" identification [99]..

4. **Uncertainty and Spatial Variability (Objective 4):**

− Voxel-wise uncertainty maps highlighted zones ($\sigma(\nu) > 0.06$) near faults and inter-well gaps [100].

− Incorporation of uncertainty directly into planning enables conservative well designs and targeted data-gathering campaigns [101].

6.2. Field Development Recommendations

1. **Drilling & Completion Design:**

− Prioritize well trajectories through zones where E > 8 GPa and UCS > 30 MPa, as indicated in the 3D model, to minimize wellbore instability risks [102].

− In high-uncertainty areas ($\sigma(\nu) > 0.04$), adopt narrower mud weight windows and conservative ramp-up rates to mitigate collapse or fracturing [103].

2. **Data Acquisition Strategy:**

− Acquire sidewall cores or dedicated coring runs in high-uncertainty fault blocks to refine calibration and reduce variance [104].

− Employ image logs (e.g., FMI) in appraisal wells to validate fracture orientation and improve geomechanical modeling inputs [105].

3. **Workflow Integration:**

− Institutionalize the ML-geomechanics workflow in real-time drilling support, updating models as new log and seismic data become available [106].

− Establish a central database for incoming logs, core results, and seismic inversion outputs to facilitate continuous model retraining [107].

6.3. Future Research Directions

- **Model Generalization:** Apply and recalibrate the workflow to adjacent deepwater blocks (e.g., OML 128/129) to test transferability and basin-wide applicability [108].
- **Advanced Uncertainty Quantification:** Explore Bayesian Neural Networks or Gaussian Process Regression to provide probabilistic property fields with inherent model-form uncertainty [109].
- **Enhanced Seismic Attributes:** Integrate broadband or multi-azimuth seismic data and attribute derivatives (e.g., curvature, anisotropy) to capture fine-scale mechanical heterogeneity [110].
- **Coupled Reservoir-Geomechanical Simulation:** Incorporate dynamic reservoir simulation to assess production-induced stress changes and subsidence over time, closing the loop between geomechanics and flow performance [111].

6.4. Future Recommendations

• Implement the ML–geomechanics workflow in real-time drilling support to enable model updates as new log and seismic data are acquired.

• Acquire additional sidewall cores and image logs in high-uncertainty fault blocks to improve calibration and reduce prediction variance.

• Extend the workflow to adjacent blocks and perform transferability tests to evaluate basin-scale applicability.

• Integrate coupled reservoir–geomechanical simulations to assess production-induced stress changes and operational risks over reservoir life.

By fulfilling the initial research objectives and offering a clear path forward, this work provides a scalable, cost-effective framework for geomechanical characterization in deepwater settings. Adoption of these recommendations will enhance drilling safety, optimize completion designs, and improve long-term reservoir management in the Agbami Field and similar offshore environments.

Declarations

Source of Funding

This study received no specific grant from any funding agency in the public, commercial, or not-for-profit sectors.

Competing Interests Statement

The authors declare that they have no competing interests related to this work.

Consent for publication

The authors declare that they consented to the publication of this study.

Authors' contributions

Both the authors took part in literature review, analysis, and manuscript writing equally.

Availability of data and materials

Supplementary information is available from the authors upon reasonable request.

Ethical Approval

Not applicable for this study.

Institutional Review Board Statement

Not applicable for this study.

Informed Consent

Not applicable for this study.

References

[1] Aigbedion, I., & Iyayi, S.E. (2007). Formation Evaluation of Oml 123 Field, Offshore Niger Delta, Nigeria. Petroleum Technology Development Journal, 2(1): 21–32.

[2] Akhundi, H., Ghafoori, M., & Lashkaripour, G.R. (2014). Prediction of shear wave velocity using artificial neural network technique, multiple regression and petrophysical data: a case study in Asmari reservoir (SW Iran). Open Journal of Geology, 4(7): 303–313. https://doi.org/10.4236/ojg.2014.47024.

[3] Ashraf, U., Zhang, H., Anees, A., Mangi, H.N., Ali, M., Zhang, X., & Tan, S. (2021). A core logging, machine learning and geostatistical modeling interactive approach for subsurface imaging of lenticular geobodies in a clastic depositional system, SE Pakistan. Natural Resources Research, 30(3): 2807–2830. https://doi.org/10.1007/s11053-021-09838-0.

[4] Bianlong, Z., Ma, D., Li, L., & Juncheng, H. (2013). Application of Logging Data in Predicting Sand Production in Oil field. Egyptian Journal of Petroleum, 22(1): 6170. https://doi.org/10.1016/j.ejpe.2012.11.008.

[5] Brocher, T.M. (2005). Empirical relations between elastic wavespeeds and density in the Earth's crust. Bulletin of the Seismological Society of America, 95(6): 2081–2092. https://doi.org/10.1785/0120050077.

[6] Brocher, T.M. (2008). Key elements of regional seismic velocity models for long period ground motion simulations. Journal of Seismology, 12(2): 217–221. https://doi.org/10.1007/s10950-007-9061-3.

[7] Carmichael, R.S. (1982). Handbook of Physical Properties of Rocks: Volume II. CRC Press.

[8] Chang, C., Zoback, M.D., & Khaksar, A. (2006). Empirical relations between rock strength and physical properties in sedimentary rocks. Journal of Petroleum Science and Engineering, 51(3–4): 223–237. https://doi.org/10.1016/j.petrol.2006.01.003.

[9] Avseth, P., Mukerji, T., & Mavko, G. (2005). Quantitative Seismic Interpretation. Cambridge University Press. https://doi.org/10.1017/cbo9780511600074.

[10] Breiman, L. (2001). Random Forests. Machine Learning, 45(1): 532. https://doi.org/10.1023/a:1010933404324.

[11] Haykin, S. (2009). Neural Networks and Learning Machines (3rd Eds.). Pearson Education.

[12] Zoback, M.D. (2007). Reservoir Geomechanics. Cambridge University Press. https://doi.org/10.1017/cbo9780511586477.

[13] Jaeger, J.C., Cook, N.G.W., & Zimmerman, R.W. (2007). Fundamentals of Rock Mechanics (4th Eds.). Blackwell Publishing.

[14] Biot, M.A. (1941). General Theory of Three-Dimensional Consolidation. Journal of Applied Physics, 12(2): 155–164. https://doi.org/10.1063/1.1712886.

[15] Hoek, E., & Brown, E.T. (1980). Empirical strength criterion for rock masses. Journal of the Geotechnical Engineering Division, 106(gt9): 1013–1035.

[16] McNally, G.H. (1987). Estimation of coal measures rock strength using sonic and neutron logs. Geo exploration, 24(4–5): 381–395. https://doi.org/10.1016/0016-7142(87)90008-0.

[17] Murphy, W.F. (1982). Effects of microstructure and pore fluids on the acoustic properties of granular sedimentary materials. Ph.D. Thesis, Stanford University.

[18] Fjær, E., Holt, R.M., Horsrud, P., Raaen, A.M., & Risnes, R. (2008). Petroleum Related Rock Mechanics (2nd Eds.). Elsevier Press. https://doi.org/10.1017/cbo9780511626753.

[19] Russell, B.H. (1988). Introduction to Seismic Inversion Methods. Society of Exploration Geophysicists. https://doi.org/10.1190/1.9781560802303.

[20] Stewart, R.R., Gaiser, J.E., Brown, R.J., & Lawton, D.C. (2002). Converted-wave seismic exploration: Methods. Geophysics, 67(5): 1348–1363. https://doi.org/10.1190/1.1512781.

[21] Goodway, B., Chen, T., & Downton, J. (1997). Improved AVO fluid detection and lithology discrimination using Lamé petrophysical parameters; "λρ", "μρ", & "λ/μ fluid stack", from P and S inversions. SEG Technical Program Expanded Abstracts, Pages 183–186. https://doi.org/10.1190/1.1885795.

[22] Chopra, S., & Marfurt, K.J. (2007). Seismic Attributes for Prospect Identification and Reservoir Characterization. SEG Geophysical Developments Series No. 11.

[23] Srivastava, N., Hinton, G., Krizhevsky, A., Sutskever, I., & Salakhutdinov, R. (2014). Dropout: A Simple Way to Prevent Neural Networks from Overfitting. Journal of Machine Learning Research, 15(56): 1929–1958.

[24] Liaw, A., & Wiener, M. (2002). Classification and Regression by random Forest. R News, 2(3): 18–22.

[25] Hastie, T., Tibshirani, R., & Friedman, J. (2009). The Elements of Statistical Learning: Data Mining, Inference, and Prediction (2nd Eds.). Springer. https://doi.org/10.1007/978-0-387-84858-7.

[26] Brown, A.R. (2011). Interpretation of Three-Dimensional Seismic Data (7th Eds.). Society of Exploration Geophysicists and American Association of Petroleum Geologists. https://doi.org/10.1190/1.9781560802884.

[27] Pyrcz, M.J., & Deutsch, C.V. (2014). Geostatistical Reservoir Modeling (2nd Eds.). Oxford University Press.

[28] Guyon, I., & Elisseeff, A. (2003). An Introduction to Variable and Feature Selection. Journal of Machine Learning Research, 3: 1157–1182.

[29] Kohavi, R. (1995). A Study of Cross-Validation and Bootstrap for Accuracy Estimation and Model Selection. Proceedings of the 14th International Joint Conference on Artificial Intelligence (IJCAI), Pages 1137–1143.

[30] Bergstra, J., & Bengio, Y. (2012). Random Search for Hyper-Parameter Optimization. Journal of Machine Learning Research, 13(10): 281–305.

[31] Neal, R.M. (2012). Bayesian Learning for Neural Networks. Springer Science & Business Media. https://doi.org/10.1007/978-1-4612-0745-0.

[32] Deutsch, C.V., & Journel, A.G. (1998). GSLIB: Geostatistical Software Library and User's Guide (2nd Eds.). Oxford University Press.

[33] Doyen, P.M. (2007). Seismic Reservoir Characterization: An Earth Modelling Perspective. SAGE Publications. https://doi.org/10.3997/9789073781746.

[34] Zoback, M.D. (2007). Reservoir Geomechanics. Cambridge University Press. https://doi.org/10.1017/cbo9780511586477.

[35] Corredor, F., Shaw, J.H., & Bilotti, F. (2005). Structural styles in the deep-water fold and thrust belts of the Niger Delta. AAPG Bulletin, 89(6): 753–780. https://doi.org/10.1306/02170504074.

[36] Yilmaz, Ö. (2001). Seismic Data Analysis (2nd Eds.). SEG. https://doi.org/10.1190/1.9781560801580.

[37] Schlumberger (2019). TechLog Wellbore Software Platform: Geomechanics Module User Guide.

[38] Ellis, D.V., & Singer, J.M. (2007). Well Logging for Earth Scientists (2nd Eds.). Springer. https://doi.org/10.1007/978-1-4020-4602-5.

[39] ASTM International (2014). ASTM D7012-14e1: Standard Test Methods for Compressive Strength and Elastic Moduli of Intact Rock Core Specimens under Varying States of Stress and Temperatures. ASTM.

[40] Hardage, B.A. (2000). Vertical Seismic Profiling: Principles (3rd Eds.). Pergamon.

[41] Hampson-Russell (2018). AVO Theory and Modeling Guide. CGG.

[42] Schlumberger (2020). TechLog 2020.2 Documentation: Depth Matching Workflows.

[43] Schlumberger (2002). SNUPAR Theory and Application. Document SMP-7025.

[44] Asquith, G., & Krygowski, D. (2004). Basic Well Log Analysis (2nd Eds.). AAPG Methods 16.

[45] Wang, Z. (2000). Dynamic versus static elastic properties of reservoir rocks. Seismic and Acoustic Velocities in Reservoir Rocks, 3: 531–539.

[46] Wang, Z. (2000). The Gassmann equation revisited: Comparing laboratory data with Gassmann's predictions. Seismic and Acoustic Velocities in Reservoir Rocks, 3: 8–23.

[47] Plumb, R.A. (1994). Influence of composition and texture on the failure properties of clastic rocks. Rock Mechanics and Rock Engineering, 27(1): 1–21. https://doi.org/10.1007/bf01020276.

[48] Dubrule, O. (2003). Geostatistics for Seismic Data Integration in Earth Models. SEG/EAGE.

[49] James, G., Witten, D., Hastie, T., & Tibshirani, R. (2013). An Introduction to Statistical Learning: with Applications in R. Springer. https://doi.org/10.1007/978-1-4614-7138-7.

[50] Chollet, F., et al. (2015). Keras. GitHub repository. https://github.com/fchollet/keras.

[51] Pedregosa, F., Varoquaux, G., Gramfort, A., Michel, V., Thirion, B., Grisel, O., & Duchesnay, É. (2011). Scikit-learn: Machine Learning in Python. Journal of Machine Learning Research, 12: 2825–2830.

[52] van der Walt, S., Schönberger, J.L., Nunez-Iglesias, J., Boulogne, F., Warner, J.D., Yager, N., & Yu, T. (2014). Scikit-image: image processing in Python. PeerJ, 2: e453. https://doi.org/10.7717/peerj.453.

[53] Goovaerts, P. (1997). Geostatistics for Natural Resources Evaluation. Oxford University Press.

[54] Hoek, E., & Diederichs, M.S. (2006). Empirical estimation of rock mass modulus. International Journal of Rock Mechanics and Mining Sciences, 43(2): 203215. https://doi.org/10.1016/j.ijrmms.2005.06.005.

[55] Horsrud, P. (2001). Estimating mechanical properties of shale from empirical correlations. SPE Drilling & Completion, 16(02): 68–73. https://doi.org/10.2118/56017-pa.

[56] Horsrud, P. (2001). Estimating mechanical properties of shale from empirical correlations. SPE Drilling & Completion, 16(02): 68–73. https://doi.org/10.2118/56017-pa.

[57] Validation split methodology - See [49].

[58] Friedman, J.H. (2001). Greedy function approximation: A gradient boosting machine. Annals of Statistics, 29(5): 1189–1232.

[59] SGS implementation - See [32].

[60] Ringrose, P., & Bentley, M. (2015). Reservoir Model Design. Springer. https://doi.org/10.1007/978-94-007-5497-3.

[61] Caers, J. (2005). Petroleum Geostatistics. SPE Textbook Series Vol. 9.

[62] Moos, D., Peska, P., & Ward, C. (2003). Wellbore Stability Analysis for Drilling. American Association of Drilling Engineers.

[63] Asef, M.R., & Farrokhrouz, M. (2017). Shale Engineering. CRC Press.

[64] Le Cun, Y., Bengio, Y., & Hinton, G. (2015). Deep learning. Nature, 521(7553): 436–444. https://doi.org/10.1038/nature14539.

[65] Pyrcz, M.J., & Deutsch, C.V. (2014). Geostatistical Reservoir Modeling (2nd Eds.). OUP.

[66] Bemis, S.P., Micklethwaite, S., Turner, D., James, M.R., Akciz, S., Thiele, S.T., & Bangash, H.A. (2011). Geologic framework of the 2010 Gulf of Mexico Oil Spill. GSA Today, 21(10): 4–10. https://doi.org/10.1130/g125a.1.

[67] Chang, C., Zoback, M.D., & Khaksar, A. (2006). Empirical relations between rock strength and physical properties in sedimentary rocks. Journal of Petroleum Science and Engineering, 51(3–4): 223–237. https://doi.org/10.1016/j.petrol.2006.01.003.

[68] Mavko, G., Mukerji, T., & Dvorkin, J. (2009). The Rock Physics Handbook (2nd Eds.). CUP. https://doi.org/10.1017/cbo9780511626753.

[69] Goodway, B., Chen, T., & Downton, J. (1997). Improved AVO fluid detection and lithology discrimination using Lamé parameters. SEG Technical Program, Pages 183–186.

[70] Bhattacharya, S., & Mishra, S. (2018). Applications of machine learning for facies and property prediction. Interpretation, 6(3): se175–se183. https://doi.org/10.1190/int-2017-0189.1.

[71] Stow, D.A.V., & Mayall, M. (2000). Deep-water sedimentary systems. Journal of the Geological Society, 157(6): 1257–1272. https://doi.org/10.1144/jgs.157.6.1257.

[72] Zhang, J., & Bentley, L.R. (2005). Factors determining Poisson's ratio in reservoir rocks. Journal of Geophysics and Engineering, 2(1): 23–34.

[73] Ottesen, S. (2018). Managed Pressure Drilling. Gulf Professional Publishing.

[74] White, A.J., Traugott, C.O., & Swarbrick, R.E. (2002). The use of leak-off tests as means of predicting minimum in-situ stress. Petroleum Geoscience, 8(2): 189–193.

[75] Hale, D. (2013). Methods to compute fault images, extract fault surfaces, and estimate fault throws from 3D seismic images. Geophysics, 78(2): o33–o43.

[76] Willigers, B.J.A., Bratvold, R.S., & Bickel, J.E. (2011). Value of information analysis for appraisal wells. SPE Economics & Management, 3(2): 75–88. https://doi.org/10.2118/138765-pa.

[77] Aminzadeh, F., & De Groot, P. (2006). Neural Networks and Other Soft Computing Techniques. SEG.

[78] Santarelli, F.J., Marsala, A.F., Brignoli, M., Rossi, E., & Bona, N. (1998). Core quality: Quantification of coring-induced rock alteration. In Rock Mechanics in Petroleum Engineering, Pages 367–376, Society of Petroleum Engineers.

[79] Lazaratos, S. (2006). Spectral shaping for seismic resolution enhancement. SEG Technical Program.

[80] Oloruntobi, O., & Butt, S. (2020). Machine learning application in reservoir characterization. Journal of Petroleum Science and Engineering, 190: 107112. https://doi.org/10.1016/j.petrol.2020.107112.

[81] Neal, R.M. (2012). Bayesian Learning for Neural Networks. Springer.

[82] Sayers, C.M. (2010). Geophysics Under Stress. SEG Geophysical Developments 11.

[83] Ma, Y.Z. (2019). Quantitative Geosciences: Data Analytics, Machine Learning & Uncertainty. Springer.

[84] Mc Nally, G.H. (1987). Estimation of coal measures rock strength using sonic and neutron logs. Geo exploration, 24(4–5): 381–395. https://doi.org/10.1016/0016-7142(87)90008-0.

[85] Dramsch, J.S. (2020). 70 years of machine learning in geoscience in review. Advances in Geophysics, 61: 1–55. https://doi.org/10.1016/bs.agph.2020.08.002.

[86] Breiman, L. (2001). Random forests. Machine Learning, 45(1): 5–32. https://doi.org/10.1023/a:1010933404324.

[87] Doyen, P.M. (2007). Seismic Reservoir Characterization. SAGE. https://doi.org/10.3997/9789073781746.

[88] Hart, B.S. (2008). Stratigraphically significant attributes. The Leading Edge, 27(3): 320–324.

[89] Deutsch, C.V., & Journel, A.G. (1998). GSLIB: Geostatistical Software Library (2nd Eds.). OUP.

[90] Willson, S.M., et al. (1999). Wellbore stability challenges in deepwater environments. SPE 52864.

[91] McLean, M.R., & Addis, M.A. (1990). Wellbore stability analysis. SPE Annual Technical Conference, SPE 19942.

[92] Zoback, M.D., Barton, C.A., Brudy, M., Castillo, D.A., Finkbeiner, T., Grollimund, B.R., Moos, D.B., Peska, P., Ward, C.D., & Wiprut, D.J. (2003). Determination of stress orientation and magnitude in deep wells. International Journal of Rock Mechanics and Mining Sciences, 40(7–8): 1049–1076. https://doi.org/10.1016/j.ijrmms.2003.07.001.

[93] Plumb, R.A., Evans, K.F., & Engelder, T. (2000). Mechanical properties test program. SPE Drilling & Completion, 15(3): 187–194. https://doi.org/10.2118/63797-pa.

[94] Barton, C.A., Tessler, R., & Moos, D. (1997). Characterizing in situ stress domains at the wellbore. SPE Annual Technical Conference and Exhibition, San Antonio, Texas, SPE-38710-MS. https://doi.org/10.2118/38710-ms.

[95] Bhattacharya, S., Ghahfarokhi, P.K., Carr, T., & Pantaleone, S. (2021). Machine learning in drilling. Journal of Petroleum Technology, 73(5): 41–43. https://doi.org/10.2118/0521-0041-jpt.

[96] Sagi, O., & Rokach, L. (2018). Ensemble learning: A survey. WIREs Data Mining, 8(4): e1249. https://doi.org/10.1002/widm.1249.

[97] Reijers, T.J.A. (2011). Stratigraphy and sedimentology of the Niger Delta. Geologos, 17(3): 133–162.

[98] Bishop, C.M. (2006). Pattern Recognition and Machine Learning. Springer.

[99] Chopra, S., & Marfurt, K.J. (2018). Seismic attributes for prospect identification. Interpretation, 6(3): 1–20.

[100] Settari, A., & Walters, D.A. (2001). Advances in coupled geomechanical and reservoir modeling. SPE Journal, 6(03): 228–239.